Fibers and Polymers 2021, Vol.22, No.1, 59-68
DOI 10.1007/s12221-021-0196-6

ISSN 1229-9197 (print version)
ISSN 1875-0052 (electronic version)

Extraction of Cellulose Nanofibrils with Ultraviolet Blocking from Agro-industrial Wastes: A Comparative Study

Xin Zhao[1], Fangchao Cheng[2], and Yingcheng Hu[1]*

[1]*Key Laboratory of Bio-based Material Science and Technology of the Ministry of Education of China, College of Material Science and Engineering, Northeast Forestry University, Harbin 150040, China*
[2]*Key Laboratory of Forestry Science and Engineering, College of Forestry, Guangxi University, Nanning 530004, China*
(Received February 22, 2020; Revised April 2, 2020; Accepted April 12, 2020)

Abstract: Cellulose nanofibrils (CNFs) were successfully isolated from agro-industrial waste (cornstalk, corn flesh, and corncob) by subjecting the raw materials to organosolv and peroxide treatment, followed by ultrasonication. A detailed comparative study was performed. Characterization results showed that the CNFs from cornstalk (CS) exhibited higher yield and lignin content (20.81 %), compared with CNFs from corn flesh (CF) and corncob (CC). The CNFs from CF and CC exhibited similar morphology, particle size, crystallinity, and thermal stability but showed improved ultraviolet blocking ability and optical transparency relative to those of CS. The CNFs from CF showed higher dispersion stability and mechanical properties than those from CS and CC. Peroxide treatment negatively influenced crystallinity and thermal stability, but exerted no apparent effect on optical transparency and mechanical strength. Thus, this study demonstrates that agro-industrial wastes are sustainable resources for CNF production, which can potentially have a wide range of value-added applications. Ionic liquid-aided solvothermal treatment followed by ultrasonication is a facile and ideal method to produce CNFs with ultraviolet blocking ability.

Keywords: Cellulose nanofibrils, Agro-industrial wastes, Ultraviolet blocking, Extraction

Introduction

Non-woody biomass resources such as agricultural residues have recently received increasing attention owing to a significant amount of cellulose in these biomass materials [1]. Agricultural residues are typically characterized by low lignin content, a short growing cycle, high annual renewability, and a high annual yield of cellulose [2]. However, residues from the agricultural industry are mainly burned for energy or used for animal feed and fertilizer, which not only results in a waste of resources but is also environmentally detrimental to a certain extent. Therefore, agricultural residues need to be developed as feedstock to produce high value-added products. Moreover, corn is one of the most abundant crops worldwide, and the yield gradually increases annually [3]. Thus, agricultural residues associated with the corn industry are considered as promising biomass materials for the development of high-value products, such as cellulose nanofibrils (CNFs) [4].

CNFs have high modulus of elasticity, large surface area, renewability, biocompatibility, biodegradability, and low density [5]. Owing to their distinctive properties and nanoscale effects, CNFs are widely used in drug delivery, flexible displays, electronic components, and other fields [6,7]. Various non-woody sources have been studied for the extraction of CNFs, including corncobs [8-10], cornstalks [11], corn husk [12], corn stover [13], kenaf [14], and flax [15]. Currently, CNFs can be produced from various woody and non-woody resources by using various methods of mechanical fibrillation, such as high-speed blending [16], grinding, high-pressure homogenization [17], and high-intensity ultrasonication [18]. All mechanical disintegration processes are highly energy-consuming. Thus, various chemical pretreatment methods are adopted to facilitate the release of fibrils and reduce energy consumption. Different pretreatment and fibrillation methods result in different types of nanosized cellulose, depending on the raw material and the disintegration process [15]. However, previous research mostly focused on the extraction of lignin-free CNF and preparation of CNF-based nanofilms to achieve improved mechanical and optical properties. Sodium chlorite or sodium hypochlorite used to remove lignin causes environmental pollution and energy consumption. Thus, a method is proposed to shorten the processing of raw materials and reduce the complexity of CNF preparation, which is significant for the large-scale application of CNFs.

The potential of agricultural biomass to produce high value-added cellulose-based products needs to be clarified considering the abundant reserves of residues from the corn industry. Thus, the characteristics and properties of CNFs need to be isolated from various agricultural residues and further analyzed for the efficient comparison and exploitation of these resources. This study aimed to isolate CNFs from three waste resources (cornstalk, corn flesh, and corncob) by ionic liquid-mediated solvothermal treatment and ultrasonication. The chemical composition, morphology, crystallinity, thermal property, and dispersion stability of the CNFs, as well as their fabrication into nanofilms, were comprehensively evaluated. The results were then compared with respect to mechanical property, optical property, and ultraviolet

*Corresponding author: yingchenghu@nefu.edu.cn

blocking ability.

Experimental

Materials

Cornstalk (CS), corn flesh (CF), and corncob (CC) under 80-mesh were used as raw materials (RMs). The samples, which were collected from Inner Mongolia in China, were air-dried and stored at room temperature. 1-Butyl-3-methylimidazolium hydrogen sulfate ([Bmim][HSO_4]) was provided by Lanzhou Institute of the Chinese Academy of Sciences; 1,4-butylene glycol was purchased from Sigma-Aldrich; and sodium hydroxide (NaOH) and hydrogen peroxide (H_2O_2) were supplied by Tianjin Kermel Chemical Reagent Co., Ltd. All chemicals, which were of analytical grade, were used as received and without further purification.

Preparation of CNFs and CNF Films from Different Resources

Pulping Purification Process

Chemical purification of the cellulose tissues from three sources was performed as described in previous methods [15,19,20]. These RMs were dispersed in distilled water, stirred for 2 h at 50 ºC, and filtered to remove soluble extractives in water. The samples were then dried overnight in an oven at 60 ºC and extracted with acetone in a Soxhlet extractor at the boiling point for 6 h to remove soluble extractives in acetone. The extracted biomass was ultimately dried at 60 ºC to constant weight.

Partial delignification was performed to facilitate further nanofibrillation. The CSs, CFs, and CCs were dispersed in 1, 4-butylene glycol/water (4:1 v/v), and [Bmim][HSO_4] was used as a catalyst. The solid/liquid ratio of the RMs, solvent, and catalyst was 1:30:1 (w/v/w). The mixture was transferred into a stainless steel reactor, and treatment was performed at 200 °C for 1 h under vigorous stirring. The solid residues of the carbohydrate-rich material (CRM) were separated by vacuum filtration and further treated with a mixture solution containing 5 wt% H_2O_2 and 4 wt% NaOH. The reaction experiment was performed in a beaker at 50 °C for 90 min. After the chemical treatment, a cream-like cellulose slurry (CEL) was obtained. To avoid generating strong hydrogen bonding among cellulose nanofibers, the samples were kept in a water-swollen state during the entire chemical treatment.

CNF Preparation with Ultrasonic Fibrillation

The CRM and CEL samples were soaked in distilled water with a concentration of 0.5 wt%. The cellulose solution was then sonicated for 20 min by using an ultrasonic processor ((JY99-IIDN, Ningbo Scientz Biotechnology Co., Ltd., China) at 20 kHz and an output power of 400 W, producing CNFs referred to in this study as UC samples including UC-CS, UC-CF, UC-CC and UBC samples including UBC-CS, UBC-CF, UBC-CC. The yield was calculated as the weight percentage of the oven-dried samples to the oven-dried raw materials.

Preparation of CNF Films

Each 5 m*l* of 0.5 wt% suspension of CNFs samples was filtrated using a filter membrane (pore size: 0.22 μm). Then, the obtained wet gel sheets were sandwiched between two filter membranes and pressed with a weight, and oven dried at 60 °C for 8 h to achieve thin films.

Characterization

Lignin Content Determination

To determine the lignin content of a sample [15,21], 0.1 g of the sample was treated with 2 m*l* of 72 wt% H_2SO_4 for 4 h at room temperature. The solution was refluxed for 2 h after 56 m*l* of H_2O was added. Kraft lignin was weighed after drying. All experiments were performed in duplicate, and their average was calculated.

Fourier Transform-infrared Spectroscopy

The chemical composition of the sample was analyzed in the 650-4000 cm^{-1} range with a resolution of 4 cm^{-1} by using an ATR-FTIR Nicolet 6700 spectrometer (Thermo Fisher Scientific Corp., USA).

Scanning Electron Microscopy

The samples were coated with gold by using a vacuum sputter coater, and imaging was conducted on a field emission scanning electron microscope (JSM-7500F, Japan) at low acceleration voltages (5-15 kV).

Transmission Electron Microscopy

Drops of cellulose nanofibrils suspension were deposited on a carbon-coated grid by using a pipette and then negatively stained in a 1 wt% solution of phosphotungstic acid to enhance the contrast of the image. After the specimen was completely dried, it was observed using a transmission electron microscope (JEM-2100, JEOL, Japan) at an accelerating voltage of 80 kV. The dimensions of the imaged nanocellulose were determined from at least 100 measurements by using the software Nano Measurer 1.2.5 (Fudan University, China). The particle size distribution percentage was calculated as the count in a certain range to the total numbers.

X-ray Diffraction

The crystallinity of the cellulose samples was determined by X-ray diffraction (D/max 2200, Rigaku, Japan) with Ni-filtered Cu Kα radiation (λ=0.154 nm) at 40 kV and 30 mA. The diffraction data were collected from 2θ=5 °-40 ° at a scanning rate of 4° min^{-1}. The relative crystallinity index of the samples was calculated using equation (1), as follows:

$$\mathrm{CrI} = \frac{I_{002} - I_{am}}{I_{002}} \times 100\% \quad (1)$$

where *CrI* is the relative crystallinity index, I_{002} is the maximum intensity of the diffraction from the 002 plane, and I_{am} is the diffraction intensity of the amorphous fraction.

Thermogravimetric Analysis

Thermogravimetric analysis (TGA) was conducted to

compare the degradation characteristics of the samples. The thermal stability of the dried samples was analyzed using a thermogravimetric analyzer (STA 6000, Perkin Elmer, USA). The samples were heated at temperatures varying from room temperature to 800 ºC at a heating rate of 10 ºC/min under a nitrogen atmosphere with a gas flow rate at 20 ml/min.

Ultraviolet-visible Spectroscopy

The transparency of the obtained nanofilms was determined using a TU-1901 spectrophotometer (Beijing Purkinje General Instrument Co. Ltd., China) with a 200-800 nm scanning wavelength range.

Mechanical Testing

The tensile strength of the nanofilms was determined using an Instron 5569 universal testing machine equipped with a load cell of 200 N at a crosshead speed of 1 mm/min. The samples measured 10 mm×5 mm×0.02-0.03 mm.

Results and Discussion

Comparative Analysis of Lignin Removal Efficiency and Chemical Compositions

The previous studies have also shown that acidic ionic liquid can effectively improve the cleavage of linkage among biopolymers and speed up the deconstruction of lignin-carbohydrate complexes (LCC) by degrading part of carbohydrates [19,22]. Cellulose fibers in various forms from the three sources were analyzed by FT-IR to evaluate the effect of pretreatment methods on lignin removal efficiency and the various chemical constituents present in the fibers. Figure 1 presents the FT-IR spectra and lignin content of the isolated CNFs and the original untreated fibers. The lignin contents of CS, CF, CC were 26.28 %, 28.40 %, and 22.6 %, respectively, which were slightly higher than those previously reported in the literature [10,13]. All types of UC and UBC showed typical cellulose structural characteristics at 3300-3340 cm^{-1} attributed to the -OH groups, 2900 cm^{-1} attributed to the C-H stretching vibration, and 890-896 cm^{-1} associated with cellulose β-glycosidic linkages [23]. These findings indicated that organic solvent and peroxide treatment caused no change in the main structure of the cellulose. The UC samples showed an absorption peak at 1735 cm^{-1} associated with C=O stretching from the ester group present in hemicellulose [24]; however, no such peak was observed in the UBC samples after hydrogen peroxide treatment. In addition, a peak at 1510 cm^{-1}, attributed to aromatic skeletal vibrations, appeared in the UC spectrum [10], indicating that lignin could not be completely removed by chemical pretreatment. The lignin contents of UC-CS, UC-CF, and UC-CC were

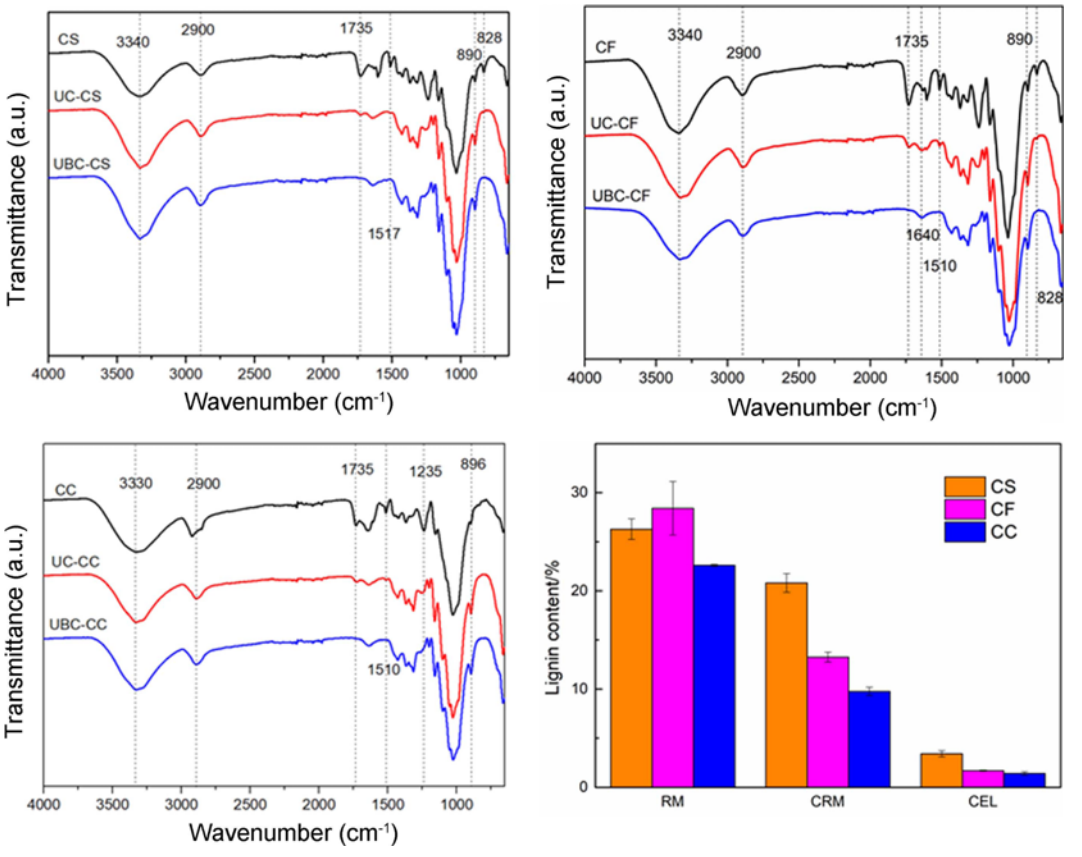

Figure 1. FT-IR spectra and lignin contents of the RM, UC, and UBC.

20.81 %, 13.25 %, and 9.77 %, respectively. The absorption peaks at 1510 cm^{-1} associated with aromatic skeletal vibrations and those at 828 cm^{-1} attributed to aromatic C-H out-of-plane bending vibrations in lignin disappeared from the spectra of UBC [25]. This observation suggested the removal of residual lignin after the hydrogen peroxide treatment. The lignin contents of UBC-CS, UBC-CF, and UBC-CC were 3.42 %, 1.70 %, and 1.42 %, respectively. Generally, treatment with organic solvent and hydrogen peroxide effectively removed nonfibrous materials but varied in lignin removal efficiency. The lignin removal efficiencies of the CF and CC samples were significantly higher than those of the CS samples under organic solvent treatment, which could be attributed to the large difference in the structure of the raw materials. The CS sample exhibited a hierarchical structure (Figure S1), hence the difficulty of chemical treatment; the sample showed a sheet structure; and the CF sample exhibited a spherical structure (Figure S1), which eased chemical processing because of its non-compact hierarchical structure .

X-ray Diffraction Analysis

Compared with non-cellulosic components such as lignin and hemicellulose, cellulose has a more distinct crystal structure mainly owing to strong hydrogen bonding and van der Waals interactions [26]. The Crl calculated from equation (1) is crucial to mechanical and thermal properties of cellulose. The crystallinity of the raw materials and CNF samples were analyzed by XRD to gain further insights into the structural changes. The results are summarized in Figure 2. All samples had main diffraction peaks near 2θ=15.8 °, 22.2 °, 34.8 ° relative to the typical pattern of cellulose I [20]. The results indicated that chemical treatment and ultrasonication did not change the crystal type of the cellulose. CS samples showed the highest relative crystallinity among the raw material samples, which was related to the contents of the cellulose and non-cellulosic components. The *Crl* of all samples increased after organosolv treatment (Figure 2). The increase in *Crl* was mainly caused by the removal of lignin and hemicellulose, which was consistent with the FT-IR analysis and lignin content analysis (Figure 1). After peroxide treatment, the *Crl* of UBC-CS and UBC-CC slightly decreased, suggesting that peroxide might negatively affected the crystalline region of the cellulose, which was consistent with previous results in the literature [27].

Analysis of the Morphology and Size Distribution of the Obtained CNCs

Different results for the morphology and diameter size of the CNFs were received by TEM (Figure 3). The UC-CS samples (83 %) had a particle size distribution ranging from 11 nm to 30 nm, and the UC-CF (88 %) and UC-CC (87 %) samples had a particle size distribution ranging from 1 nm to

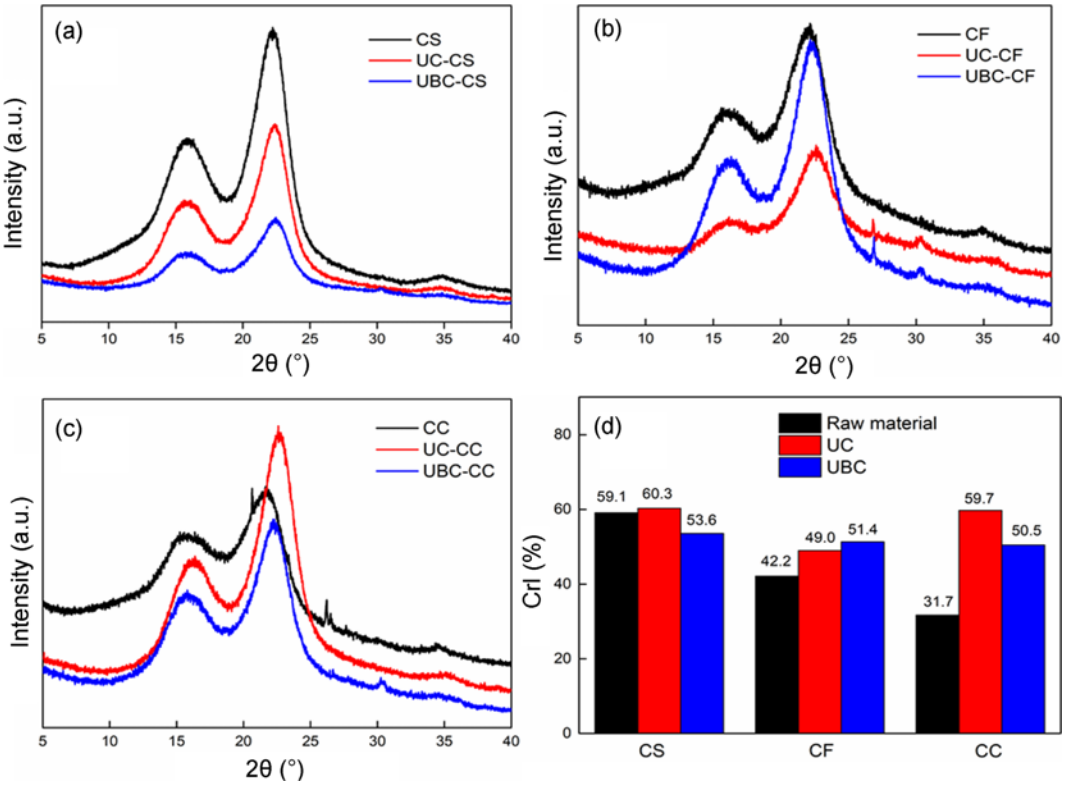

Figure 2. XRD patterns (a)-(c) and (d) Crl of RM, UC, and UBC samples.

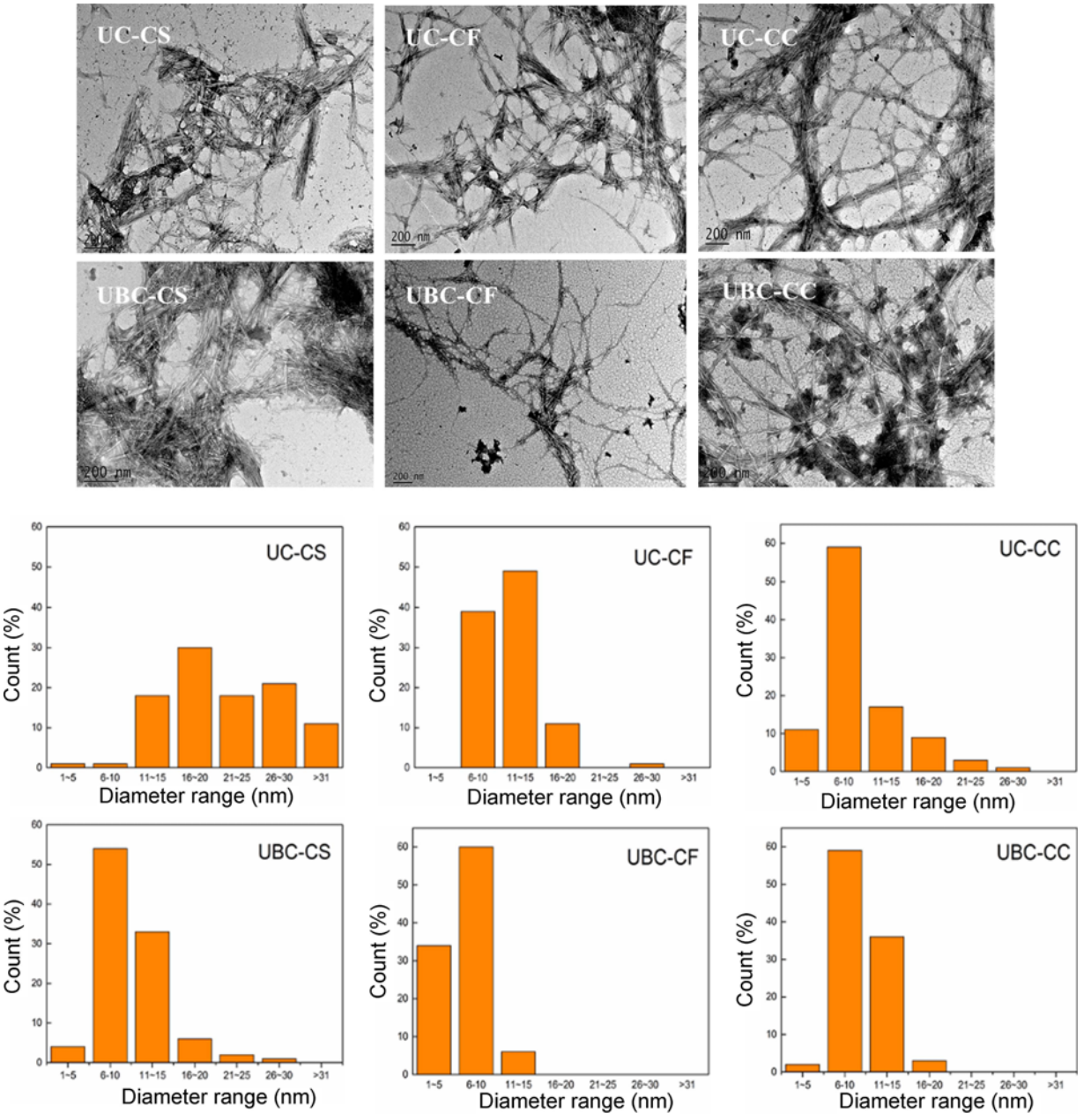

Figure 3. TEM images and Size distribution of the UC and UBC samples.

15 nm. The results indicated that some aggregates or non-disintegrated cellulose fragments were present, and the residual lignin caused the aggregation of the CNFs. The number of non-disintegrated aggregates was significantly reduced by peroxide treatment. The diameter of UBC-CS (87 %) ranged from 6 nm to 15 nm. UBC-CF (100 %) and UBC-CC (97 %) had a particle size distribution ranging from 1 nm to 15 nm. Generally, regardless of the similar conditions for ultrasonication, the size distribution varied because of the source of raw material and residual lignin content [28]. High lignin content inhibited the disintegration of cellulose fragments during ultrasonication. CNFs from CF and CC had a smaller particle size distribution.

Zeta Potential and Yield of the CNFs

The dispersion stability of CNF suspension was determined using the zeta potential. Figure 4(a) shows the zeta potential values of the CNF samples. All samples showed negative zeta potential values, which were attributed to the hydroxyl groups on the cellulose surface. The UC-CS, UBC-CS UC-CC, and UBC-CC samples showed small zeta potential values, which indicated the CNF samples with a number of

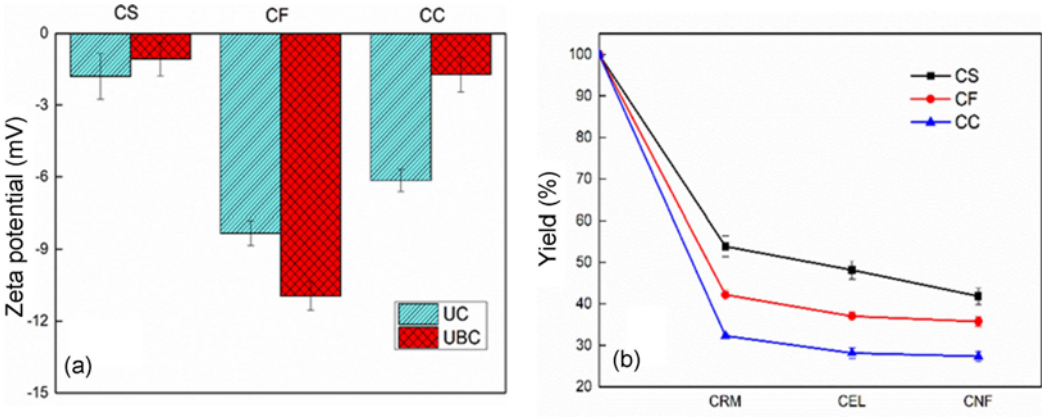

Figure 4. (a) Zeta potential of the cellulose nanofibrils suspensions and (b) yield of cellulose-rich materials during extraction of cellulose nanofibrils.

hydroxyl groups. The UBC-CF samples had the maximum zeta potential values (~11 mV) among the CNF samples, which were attributed to the lower lignin content and greater number of hydrophilic carbonyl groups resulting from the oxidation of some hydroxyl groups [7]. Such zeta potential values were also lower than those of nanocellulose produced using various extraction processes (between -15 mV and -50 mV) [29]. The CNF samples were likely to aggregate because of the weak electrostatic repulsive forces among the CNFs, which is in accordance with the observation by TEM (Figure 3).

The yield of nanocellulose is a key factor in the evaluation of the method of nanocellulose extraction. Figure 4(b) presents the yield of the cellulose-rich materials during CNF extraction. The yields of the CRM from CS, CF, and CC were 53.85 %, 42.19 %, 32.28 %, respectively. These results indicated that the yield of cellulose-rich materials decreases with the removal of hemicellulose and lignin during organosolv pretreatment. Removal of more lignin indicated greater weight loss. After peroxide treatment, the cellulose

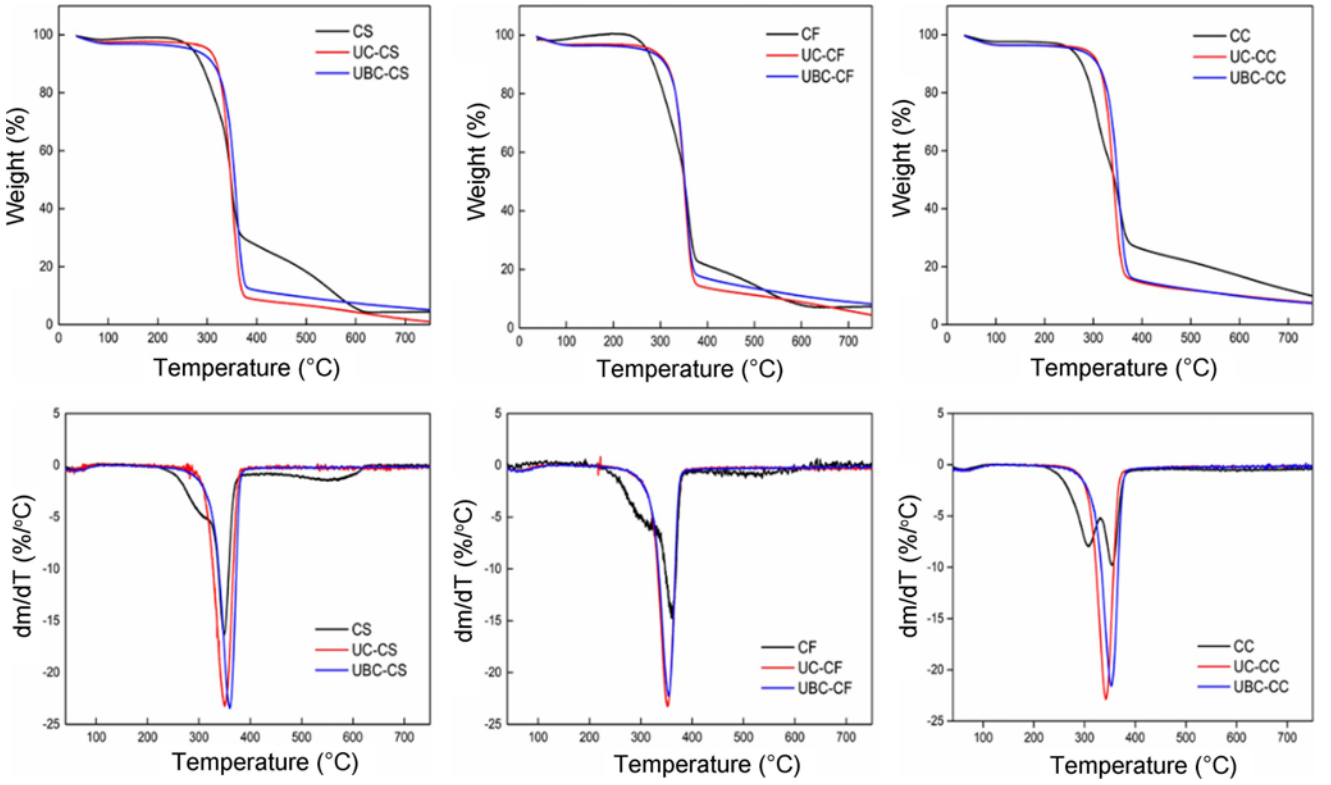

Figure 5. Thermogravimetric analysis and derivative thermogravimetric analysis curves of raw materials, UC, and UBC samples.

Table 1. T_{on} and T_{max} of the raw materials and UC and UBC samples

Sample	T_{on} (°C)[a]	T_{max} (°C)[b]	Char at 700 °C (%)
CS	258	348	4.37
UC-CS	308	350	1.92
UBC-CS	305	359	5.79
CF	253	360	7.20
UC-CF	299	351	5.92
UBC-CF	297	354	8.96
CC	262	355	11.94
UC-CC	296	341	8.31
UBC-CC	304	353	8.05

[a]Onset temperature of thermal decomposition and [b]temperature of maximum decomposition.

from CS, CF, and CC obtained yields of 48.17 %, 37.01 %, and 28.14 %, respectively, reflecting a 4-6 % decline in mass attributed to the treatment. After ultrasonication, the CNFs from CS, CF, and CC obtained yields of 41.85 %, 35.75 %, and 27.33 %, respectively, which were higher than those produced using other methods. Generally, the greater the number of pretreatment steps, the larger the decline in the yield of cellulose-rich materials, which affects the yield of nanocellulose.

Thermal Stability Analysis

TGA and derivative thermogravimetric analysis (DTGA) curves are presented in Figure 5. The onset temperature of thermal decomposition (T_{on}) and the maximum decomposition temperature (T_{max}) refer to the initial degradation temperature and the maximum rate of degradation temperature, respectively, which are summarized in Table 1. The mass loss observed around 60-105 °C of all samples is attributed to the evaporation of absorbed water on the surface. The values of the raw materials and CNF samples show a significant difference between the T_{max} of the nanoparticles and that of the raw materials.

Due to the low decomposition temperature of hemicellulose and lignin, the curve of the raw materials shows an earlier weight loss that started at around 250-260 °C, which reached the dominant peak at 348-360 °C on the DTG curve, accounting for the pyrolysis of cellulose. The CNFs samples showed a higher decomposition temperature at 297-308 °C. The higher temperature around 350 °C of thermal decomposition of CNFs is related to the partial removal of lignin and hemicellulose from the raw materials, as well as the higher crystallinity of cellulose. Besides, there is no significant difference between the T_{on} and T_{max} for the UC samples and UBC samples, which might due to the comprehensive influence of peroxide treatment on the chemical composition and crystal structure of cellulose.

Structure and Mechanical Properties of CNF Films

The assembly of CNFs depends primarily on its morphology, surface properties, and the drying process applied. A uniform structure contributes to the mechanical performance of the nanofilms. For the UC-CS nanofilms, some residual lignin and cytoderm fragments remained,

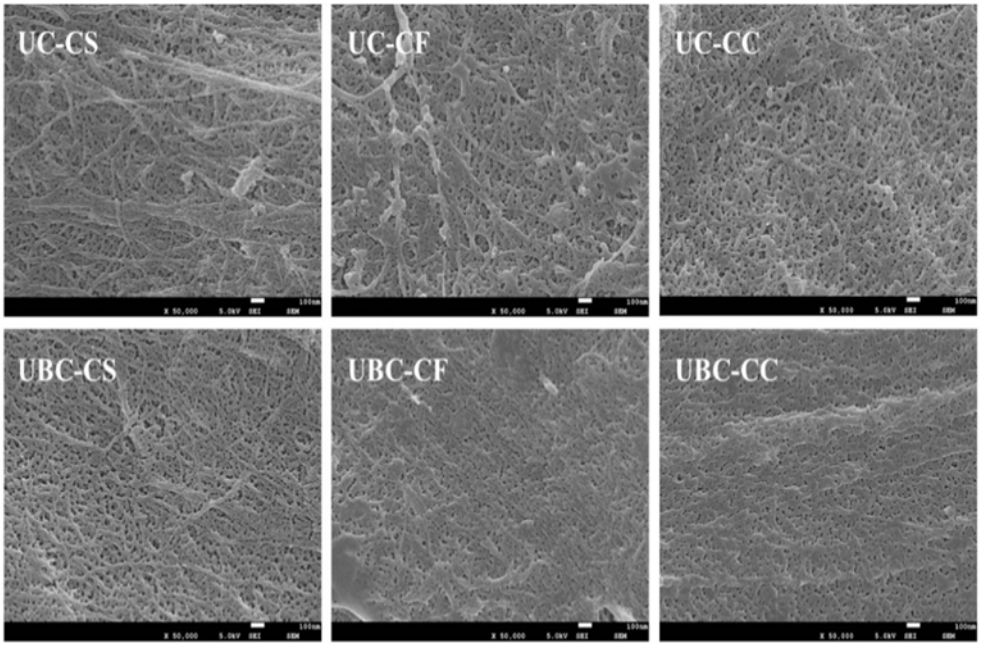

Figure 6. SEM micrographs of the CNF nanofilms at ×5000 magnification.

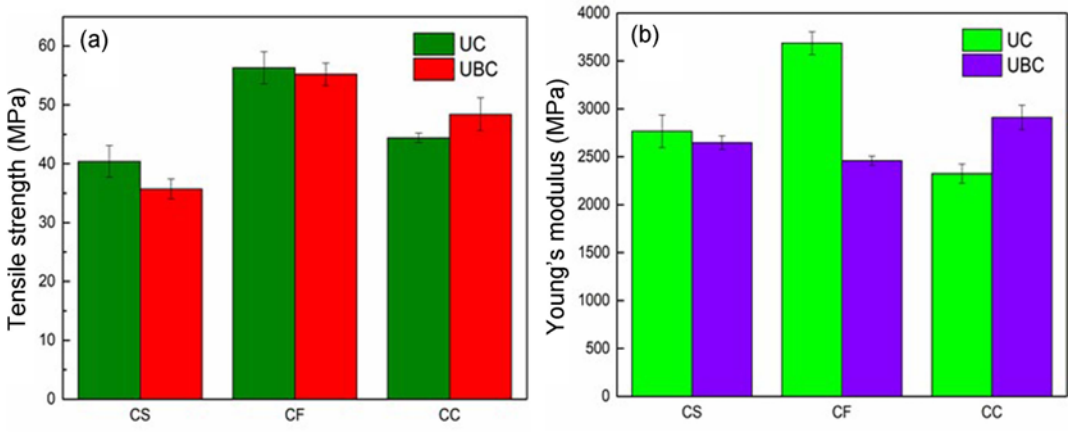

Figure 7. Tensile strength and Young's modulus of the cellulose nanofibrils; (a) tensile strength and (b) Young's modulus of the cellulose nanofibrils.

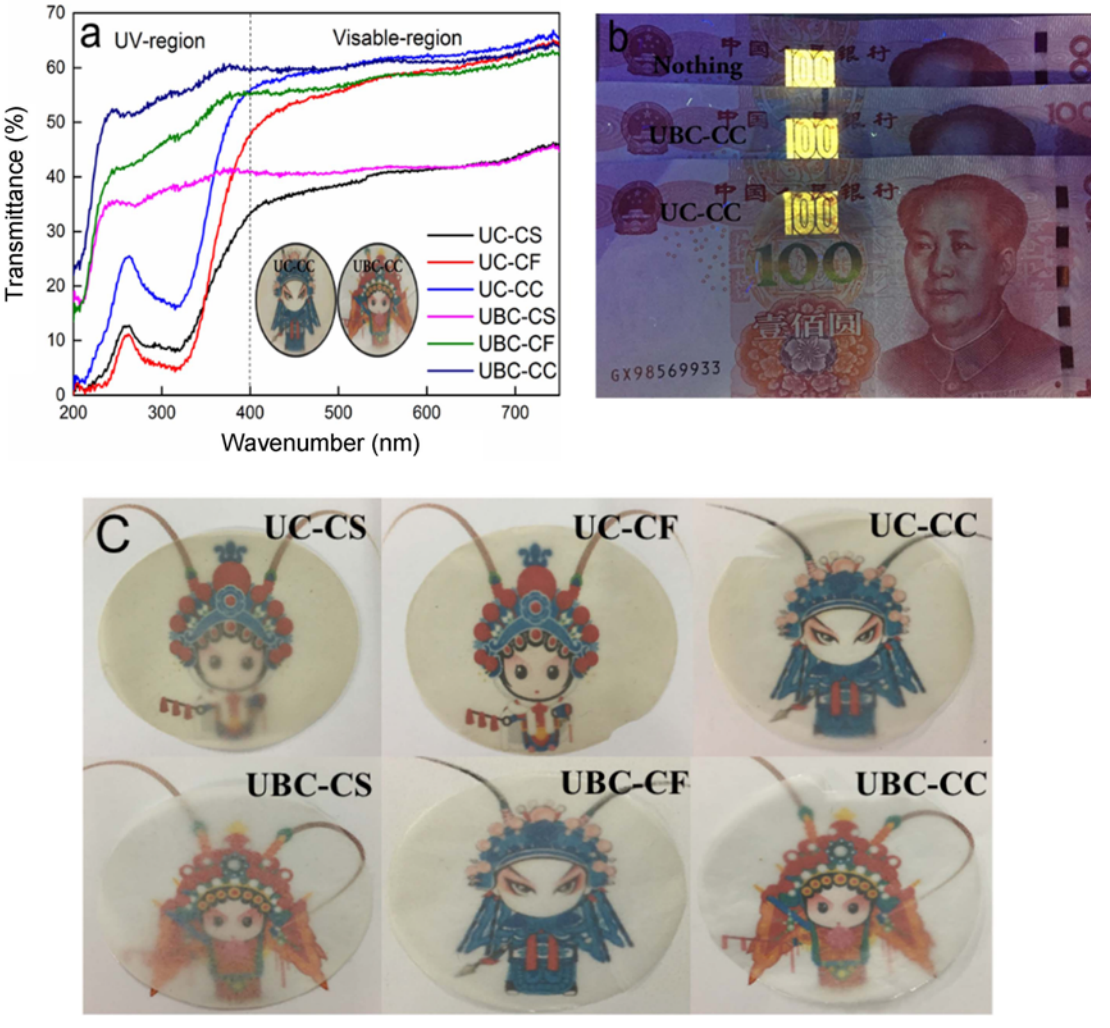

Figure 8. (a) UV-vis light transmittance spectra of UC and UBC films (b) digital photographs showing the UV-blocking performance of UBC-CC and UC-CC. Paper money without a shield, shielded by UBC-CC, shielded by UC-CC, and exposed to UV light with a wavelength of 254 nm. (c) digital photographs of CNF films.

causing surface roughness. The UC-CS nanofilm exhibited a tensile strength of 40 MPa, which was lower than those of the UC-CF and UC-CC samples. After peroxide treatment, the CS and CF nanofilms slightly decreased in tensile strength, which could be attributed to the negative effect of peroxide treatment on the crystallinity of cellulose. All samples had a Young's modulus in the 2400-3700 MPa range, which benefited their application in composite reinforcement.

Comparison of Optical Properties

Transparency and ultraviolet (UV)-blocking ability are important optical properties for the application of nanocellulose films in optoelectronics [30]. Figure 8 shows the UV-vis spectra of the UC and UBC film and the UV-blocking performance. The transmittance of visible light T(UVA) and T(UVB) was calculated using the equations reported in previous studies [31] (Table S1). UC-CC exhibited higher transmittance (62.02 %) than those of UC-CS (41.14 %) and UC-CF (58.94 %) in the visible region (l between 400 and 800 nm). The T(UVA) and T(UVB) of UC-CS were 20.44 % and 8.77 %, respectively, and those of UC-CF were 24.96 % and 5.59 %, respectively. These results indicated higher absorption of UVA (315-400 nm) and UVB (280-315 nm) of UC-CS and UC-CF than that of UC-CC, which was attributed to lignin content. The presence of UV-absorbing functional groups, such as phenolic rings, ketones, and other chromophores, in lignin provides anti-UV properties [32]. Sulfation during organosolv treatment most likely altered the light-absorbing properties of lignin, resulting in the formation of light-brown UC samples. Hydrogen peroxide as an oxidization agent exerted a more aggressive effect on lignin and hemicellulose, thereby reducing the hemicellulose and lignin contents in UBC. Therefore, the UBC samples were almost colorless. In addition, the hydrogen peroxide treatment significantly affected the transmittance of the nanofilm in the UV region but exerted no obvious effect on the transmittance of the film in the visible region. Generally, the UC samples exhibited efficient UV shielding and UC-CF showed the best transparency and UV-blocking ability.

Conclusion

Ionic liquid-catalyzed solvothermal treatment followed by ultrasonication is a suitable method to isolate CNFs with ultraviolet blocking ability from CS, CF, and CC. Comparative analysis of the composition and characteristics of the samples indicated that the yield, lignin content, crystallinity, optical transparency, and morphology were dependent on the origin of the fibers. The structure and composition affect the efficiency of the solvent system in the processing of the raw materials, resulting in different lignin content in the sample, which in turn results in different samples having different UV-blocking performance. UC-CS showed the largest lignin content and yield but exhibited poor dispersion and optical transparency among all samples. UC-CF and UC-CC showed better ultraviolet blocking ability and optical transparency than UC-CS. With regard to mechanical properties, UC-CF exhibited a higher tensile strength and Young's modulus than UC-CS and UC-CC. Thus, this study provides a method to isolate CNFs from agro-industrial materials, which is significant for improving the use of agro-industrial materials in various value-added applications.

Acknowledgements

This project was supported by the Fundamental Research Funds for the Central Universities (2572020DR13), and the National Natural Science Foundation of China (31470581).

Electronic Supplementary Material (ESM) The online version of this article (doi: 10.1007/s12221-021-0196-6) contains supplementary material, which is available to authorized users.

References

1. G. Marques, J. Rencoret, A. Gutiérrez, J. C. D. Río, and J. C. Del Río, *Open Agric. J.*, **4**, 93 (2010).
2. S. Alila, I. Besbes, M. R. Vilar, P. Mutje, and S. Boufi, *Ind. Crops Prod.*, **41**, 250 (2013).
3. C. Du, H. Li, B. Li, M. Liu, and H. Zhan, *Bioresources*, **11**, 5276 (2016).
4. F. Valdebenito, M. Pereira, G. Ciudad, L. Azocar, R. Briones, and G. Chinga-Carrasco, *Ind. Crops Prod.*, **95**, 528 (2017).
5. H. M. Ng, L. T. Sin, T. T. Tee, S. T. Bee, D. Hui, C. Y. Low, and A. R. Rahmat, *Compos. Part B-Eng.*, **75**, 176 (2015).
6. E. Lam, K. B. Male, J. H. Chong, A. C. W. Leung, and J. H. T. Luong, *Trends Biotechnol.*, **30**, 283 (2012).
7. R. J. Moon, M. Ashlie, N. John, S. John, and Y. Jeff, *Chem. Soc. Rev.*, **40**, 3941 (2011).
8. C. Liu, B. Li, H. Du, D. Lv, Y. Zhang, G. Yu, X. Mu, and H. Peng, *Carbohydr. Polym.*, **151**, 716 (2016).
9. R. L. Shogren, S. C. Peterson, K. O. Evans, and J. A. Kenar, *Carbohydr. Polym.*, **86**, 1351 (2011).
10. Silverio, H. Alves, F. Neto, W. Pires, Pasquini, Daniel, Dantas, and N. Oliveira, *Ind. Crops Prod.*, **44**, 427 (2013).
11. S. Boufi and A. Chaker, *Ind. Crops Prod.*, **93**, 39 (2016).
12. X. Yang, F. Han, C. Xu, S. Jiang, L. Huang, L. Liu, and Z. Xia, *Ind. Crops Prod.*, **109**, 241 (2017).
13. L. N. Luduena, A. Vecchio, P. M. Stefani, and V. A. Alvarez, *Fiber. Polym.*, **14**, 1118 (2013).
14. M. Jonoobi, J. Harun, P. M. Tahir, L. H. Zaini, S. Saifulazry, and M. D. Makinejad, *Bioresources*, **5**, 2556 (2010).
15. W. Chen, H. Yu, Y. Liu, Y. Hai, M. Zhang, and P. Chen, *Cellulose*, **18**, 433 (2011).

16. U. Kojiro and Y. Hiroyuki, *Biomacromolecules*, **12**, 348 (2011).
17. L. Jihua, W. Xiaoyi, W. Qinghuang, C. Jiacui, C. Gang, K. Lingxue, S. Junbo, and L. Yuhuan, *Carbohydr. Polym*., **90**, 1609 (2012).
18. W. Chen, H. Yu, Y. Liu, C. Peng, M. Zhang, and Y. Hai, *Carbohydr. Polym*., **83**, 1804 (2011).
19. F. Cheng, X. Zhao, and Y. Hu, *Bioresour Technol*, **249**, 969 (2018).
20. M. F. Rosa, E. S. Medeiros, J. A. Malmonge, K. S. Gregorski, D. F. Wood, L. H. C. Mattoso, G. Glenn, W. J. Orts, and S. H. Imam, *Carbohydr. Polym*., **81**, 83 (2010).
21. R. Li, J. Fei, Y. Cai, Y. Li, J. Feng, and J. Yao, *Carbohydr. Polym*., **76**, 94 (2009).
22. G. Feng, F. Zhen, and T. J. Zhou, *Bioresour Technol.*, **112**, 313 (2012).
23. N. Johar, I. Ahmad, and A. Dufresne, *Ind. Crops Prod*., **37**, 93 (2012).
24. J. Xu, E. F. Krietemeyer, V. M. Boddu, S. X. Liu, and W.-C. Liu, *Carbohydr. Polym*., **192**, 202 (2018).
25. Q. Wang, H. Du, F. Zhang, Y. Zhang, M. Wu, G. Yu, C. Liu, B. Li, and H. Peng, *J. Mater. Chem. A*, **6**, 13021 (2018).
26. W. Chen, H. Yu, S.-Y. Lee, T. Wei, J. Li, and Z. Fan, *Chem. Soc. Rev*., **47**, 2837 (2016).
27. Y. Li, Y. Liu, W. Chen, Q. Wang, Y. Liu, J. Li, and H. Yu, *Green Chem*., **18**, 1010 (2016).
28. F. I. Ditzel, E. Prestes, B. M. Carvalho, I. M. Demiate, and L. A. Pinheiro, *Carbohydr. Polym*., **157**, 1577 (2017).
29. Z. Pang, P. Wang, and C. Dong, *Cellulose*, **25**, 7053 (2018).
30. H. Zhu, B. B. Narakathu, Z. Fang, A. Tausif Aijazi, M. Joyce, M. Atashbar, and L. Hu, *Nanoscale*, **6**, 9110 (2014).
31. Y. Feng, J. Zhang, J. He, and J. Zhang, *Carbohydr. Polym*., **147**, 171 (2016).
32. C. Pouteau, P. Dole, B. Cathala, L. Averous, and N. Boquillon, *Polym. Degrad. Stab*., **81**, 9 (2003).